공학석사학위논문

Prediction of NOx Emissions of $H_2/CO/CH_4$ Syngas in a Model Gas Turbine Combustor using Artificial Neural Networks

인공 신경망을 이용한 모델 가스터빈 연소기에서 $H_2/CO/CH_4$ 합성가스의 NOx 배출량 예측

2014 년 2 월

서울대학교 대학원

기계항공공학부

주 성 필

Prediction of NOx Emissions of H_2/CO/CH_4 Syngas in a Model Gas Turbine Combustor using Artificial Neural Networks

지도교수 윤 영 빈

이 논문을 공학석사 학위논문으로 제출함

2013 년 12 월

서울대학교 대학원

기계항공공학부

주 성 필

주성필의 공학석사 학위논문을 인준함

2013 년 12 월

위 원 장 : _____

부위원장 : _____

위 원 : _____

Abstract

Prediction of NOx Emissions of H_2/CO/CH_4 Syngas in a Model Gas Turbine Combustor using Artificial Neural Networks

Seongpil Joo

School of Mechanical and Aerospace Engineering

The Graduate School

Seoul National University

Recently, the interests for energy depletion and rapid climate change have emerged around the world. To address the problems, the clean coal technology and research have been conducted actively. The business, which gasification accounting for a large proportion of the technology, has been performed in USA, China, Korea, etc. Gasification technology can generate synthetic gas from solid coal through carbon capture and storage technique (CCS). However, the study is not enough to investigate the combustion characteristics still.

In this study, combustion experiment was performed to investigate the combustion characteristics for H2/CO/CH4 syngas in the partially premixed model gas turbine combustor equipped GE 7EA nozzle. Chemiluminescence

measurements were performed to study the flame structure and characteristics of syngas combustion over equivalence ratio 0.7 to 1.3. Abel inversion method was applied to obtain 2-D chemiluminescence flame images from 3-D accumulated chemiluminescence image. EINOx was measured to investigate the relation with flame structure. EINOx related to the flame length and flame temperature. Artificial neural networks (ANN) process was employed to establish the EINOx prediction modeling. OH*, CH* and C_2* overlapped chemiluminescence image was more accurate to estimate the EINOx for H_2/CO/CH_4 various syngas compositions from the ANN results. As well, most effectiveness of the EINOx concentration was order of flame temperature, flame length and mass flow rate.

Keywords: Gas turbine, Artificial neural network, Chemiluminescence, Flame structure, Abel transform, EINOx

Student Number: 2012-20708

Contents

List of Tables

List of Figures

Chapter 1 INTRODUCTION

1.1 NOx (EINOx) emission

NOx is the chemical compound of the nitrogen (N) and oxide (O). They are produced from the chemical reaction of the nitrogen and oxygen gases during combustion state. Especially, they are generated more at high temperature combustions. Diatomic molecular nitrogen (N_2) makes up about 79% inert gas. However, the chemical element nitrogen (N) is very reactive level and has five ionization states (from +1 to +5). Oxygen ions are always minus 2 equilibrium state. Therefore, nitrogen can be formed several compounds. These NOx compounds can react to either deplete or enhance ozone concentrations. When the nitro-oxides dissolve in water and decompose, they form nitric acid (HNO_3) or nitrous acid (HNO_2). Nitric acid forms nitrate salts when it is neutralized. These gases, acid gases and salts contribute to pollution effects and attribute to acid rain. Besides, N_2O is a “Greenhouse gas” which, like carbon dioxide (CO_2), absorbs long wavelength infrared radiation to hold great radiating from Earth, and thereby contributes to global warming. The family of NOx compounds and their properties are listed in Table 1.1 [1].

Formula	Name	Nitrogen valence	properties
N_2O	Nitrous oxide	1	- Colorless gas - Water soluble
NO N_2O_2	Nitric oxide Dinitrogen dioxide	2	- Colorless gas - Slightly water soluble
N_2O_3	Dinitrogen trioxide	3	- Black solid - Water soluble, decomposes in water
NO_2 N_2O_4	Nitrogen dioxide Dinitrogen tetroxide	4	- Red-brown gas - Very water soluble, decomposes in water
N_2O_5	Dinitrogen pentoxide	5	- White solid - Very water soluble, decomposes in water

Table 1.1 Nitrogen Oxides (NOx)

NO is the primary form of the NOx emissions from combustions. According to the Zeldovich NOx mechanism, NO is generated to the limit of available oxygen in air at temperature above 1,300℃. At temperature below 760℃, NO is either generated in much lower concentrations or not at all. NO generation from combustion is a function of equivalence ratio and temperature. In addition, Most NO generation occurs on the fuel-lean side of the stoichiometric ratio. Because, the maximum temperature occurs not at stoichiometric, but, rather, at a slightly rich equivalence ratio (φ~1.05). That the maximum temperature is at a slightly rich equivalence ratio is a consequence of both the heat of combustion and heat capacity of the products declining beyond φ=1 [2]. Electric power plant boilers

produce about 40% of the NOx emissions from stationary sources [3]. If the NOx emissions from power plant could be reduced, atmospheric environment might be able to maintain clean.

There are three NOx chemical mechanisms in the combustion; thermal (Zeldovich mechanism) NOx, fuel NOx and prompt (Fenimore mechanism) NOx [2] and EINOx.

1. Thermal (Zeldovich mechanism) NOx

The concentration of thermal NOx is very sensitive to the local flame temperature and is formed in the post flame of the combustion. Thermal NOx is usually unimportant at temperatures below 1800K, as well. Therefore, the major parameters of thermal NOx are flame temperature, the residence time and the fuel-air mixing intensity. The Zeldovich equations are:

$$N_2+O \rightarrow NO+N \quad (1.1)$$

$$N+O_2 \rightarrow NO+O \quad (1.2)$$

$$N+OH \rightarrow NO+H \quad (1.3)$$

2. Fuel NOx

Fuel (e.g., coal and oil) may contain nitrogen up to about 2 percent by mass. In combustion, the nitrogen of the fuel react oxygen in the air rapidly. Fuel NOx composed as much as 50% of the emissions when combusting oil and as much as 80% when combusting coal. If there are no nitrogen in the fuel (e.g., synthetic gas), fuel NOx do not need to be considered.

3. Prompt (Fenimore mechanism) NOx.

The Fenimore mechanism includes the combustion chemistry of hydrocarbons. According to Fenimore mechanism, hydrocarbon radicals react with molecular nitrogen to generate HCN or CN. These compounds convert to NO. In the process, CH radical is formed to initiate the mechanism. The Fenimore mechanism can be written

$$CH+N_2 \rightarrow HCN+N \quad (1.4)$$

$$C+N_2 \rightarrow CH+N \quad (1.5)$$

$$HCN+O \rightarrow NCO+H \quad (1.6)$$

$$NCO+H \rightarrow NH+CO \quad (1.7)$$

$$NH+H \rightarrow N+H_2 \quad (1.8)$$

$$N+OH \rightarrow NO+H \quad (1.9)$$

The emission index (EI) as suggested by Turns and Lovett are used to convert the measured emission concentrations of NOx and CO. EINOx define the total grams of NOx formed per kilogram of fuel. EINOx is closely related to the flame residence time, flame structure and global strain rate. Therefore, EINOx can be indicator for the emission concentration with burnt fuel.

4. EINOx (Emission Index of NOx)

For analyzing NOx, CO and O2 emissions, TESTO 360 gas analyzer was

introduced. The TESTO 360 reference measuring system consists of an analyzer unit, a notebook and the flue gas probe. All of the sensors (max. 7 gas sensors), the flue gas moisture measurement unit (optional), the measuring range extension unit (gas dilution, optional) velocity measurement (optional) as well as a low absorption gas preparation Peltier cooling unit are located in the analyzer.

The expression for calculating EINOx follows.

$$EINOx = 0.001 X_{NOx} \left(\frac{MW_{NOx}}{MW_F}\right) \frac{\left(1+4.76/\varphi_G\right)}{2} \tag{1.10}$$

X_{NOx} is the measured concentration (ppm) of NOx, MW_{NOx} is the molecular weight of NOx, MW_F is the molecular weight of fuel and φ_G is global equivalence ratio, respectively.

1.2 Chemiluminescence

Chemiluminescence is the emissions of light. It is related with the electronically excited species. When fuel react the oxide in the flame zone, the flame emit light that is contributed by chemical reaction.

$$\text{Fuel} + \text{Oxide} \rightarrow \text{Product} + X^* \tag{1.11}$$

The excited molecule X* is produced due to non-equilibrium collision and the molecule jumps to a high energy state during chemical reaction. Then, these return to lower energy state and emit discharging energy between those. It can be destroyed by spontaneous emission or quenching collision as follows:

$$X \rightarrow X + hv \tag{1.12}$$

$$X^* + M \rightarrow X + M \tag{1.13}$$

Where, h is Planck's constant and v is the frequency of the light. When, radiations occur for the reasons of the released energy from excited state to the final state. Optical radiation from a flame related to several combustion reactions is chemiluminescence [4].

Doxquier et al. [5] addressed the most luminous excited radical s as shown in Table 1.2.

Radical	Transition	λ [nm]
OH*	$A^2\sum^+ \rightarrow X^2\prod (\Delta v=1)$	282.9
OH*	$A^2\sum^+ \rightarrow X^2\prod (\Delta v=0)$	308.9
CH*	$B^2\sum^- \rightarrow X^2\prod$	387.1
CH*	$A^2\Delta \rightarrow X^2\prod$	431.4
C_2*	$A^3\prod_g \rightarrow X^3\prod_u$ (Swan)	516.5
CO_2*	Continuum	350 ~ 500

Table 1.2 Excited radicals observed in typical flames

The wavelength of radiation is emitted that is characteristics of the particular molecule. The OH*, CH* and C_2* take spectrum with about 309nm, 431nm and 516nm respectively and CO_2* is characterized a broad emission spectrum extending from 350 to 500.

There are three chemiluminescence characteristics in the combustion as follow; OH* radical characteristics, CH* characteristics and C_2* characteristics.

1. OH* radical characteristics

OH* is a radiation emitted from electronically excited molecules. The concentration of OH* represents the equilibrium at the flame temperature. In hydrocarbon flame, the main reaction can show above equation (1.13) and represents the heat distribution of the chemical reaction [6].

$$CH + O_2 \rightarrow CO + OH^* \qquad (1.14)$$

When the premixed fuel and air flows near the flame front, the OH* radical emission reacts forward in the premixed mixtures. The spontaneous emission via the reaction is given by

$$OH^* \rightarrow OH + hv \quad (1.15)$$

hv represents one photon at about 306nm. Therefore, the OH* radical intensity is related to the main flame temperature, reaction rate and heat release rate.

2. CH* radical characteristics

CH*, exhibits a spectrum peak near 431nm, spontaneous emission via the reaction is given below equation. The reaction includes the combinations of C_2 with OH reaction.

$$C_2H + O \rightarrow CO + CH^* \quad (1.16)$$

$$C_2 + OH \rightarrow CO + CH^* \quad (1.17)$$

CH* represents a path for the reaction zone. However, CH* radical detected very low concentration compared to OH* radical. CH* radical is not a parameter for the methane combustion, but this is proper indicator of heat release for the hydrocarbon flames. In addition, CH* radical emission reacts strong in the front flame as fuel rich condition. In general, CH* radical is an important indicator of prompt NOx formation because it include Fenimore mechanism.

3. C_2* radical characteristics

The C_2* radical concentration may show a rich flame, because C_2* radical require two C radical in the reaction zone.

$$CH_2 + C \rightarrow H_2 + C_2^* \quad (1.18)$$

$$CH + C \rightarrow H + C_2^* \quad (1.19)$$

The excited C_2* radical is not a suitable indicator for the fuel lean mixture flames. If a fuel do not have C molecule such as hydrogen, C_2* would not emit during combustion.

1.3 Artificial neural network

Artificial intelligence (AI), or computational intelligence, is intelligence ascribed to a computer system, or research aiming at constructing computer systems that demonstrate intelligent behavior. The purpose is to artificially resemble a brain's capacity to draw conclusions, plan, solve problems, and learn etc. it is relatively new and the term artificial intelligence [7].

Artificial neural network (ANN) is a non-linear statistical data modeling tool mimicking the neural structure of the human brain, and it basically learns from experience or adaptive [8]. Instead of being built a priori from specification, neural and adaptive systems use external data to automatically set their parameters. ANN can be used to solve a variety of tasks, including classification, regression, general estimations problems, etc. An ANN consists of a group of interconnected artificial neurons processing information in parallel. The performance of a network can be improved by rendering it "aware" of its output(s) through a performance feedback loop that includes a cost function. The feedback is used to adjust the network parameters through systematic procedures called learning or training rules, in order to improve the system output with respect to the desired goal. The progress of learning (or training) is an iterative process and involves modifying the strength of connections between the elements.

Supervised learning is used for tasks of classification and regression, whereas unsupervised learning is more suitable for data clustering, compression and filtering tasks. There is a fundamental difference between clustering and classification: clustering represents the process of grouping input samples that are

spatial neighbors, whereas classification involves the labeling of input samples via some external criterion. Clustering is an unsupervised process of grouping, while classification is supervised.

There are several types of neural networks which can be categorized according to the topology of their connections. The two main groups are represented by feed-forward networks and recurrent (feed-back) networks (see Figure 2.4). The feed-forward network is the simplest network where information only travels in a single direction, i.e. linearly from input to output. In a recurrent network, a later processing stage can propagate signals to an earlier stage. Recurrent networks can be used for e.g. dynamic or time-dependent mapping, while a feed-forward network is used for static mapping. Since the research presented in the scientific papers concerns static mapping, the focus of this chapter is on the feed-forward network.

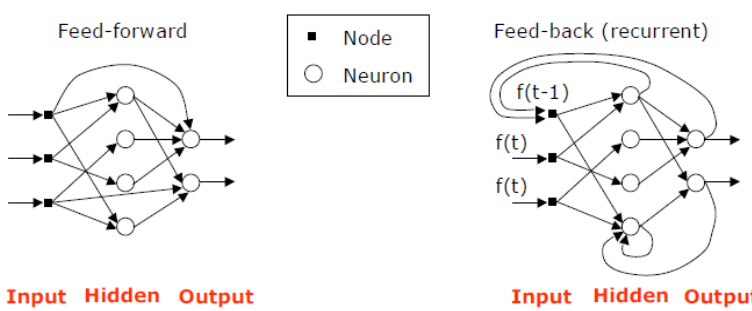

Figure 1.1 The main artificial neural network architectures [9].

Once the use of neural networks for the non-linear modeling (regression) of a system has been established, certain network specifics have to be decided on, such as these criteria: Number of hidden layers, number of neurons in hidden layers,

transfer functions in neurons, error criteria, training algorithm, stop criteria and initial values of weights [8].

1. Number of hidden layers

The number of hidden layers is decided based on trial and error. But one hidden layer is enough to approximate any continuous function, as long as the number of neurons in this hidden layer is sufficient. Additional hidden layers are seldom required for regression tasks while it might be useful for other tasks [10].

2. Number of neurons in hidden layers

The number of neurons in hidden layers is also determined through a trial and error process, normally reduced to find the appropriate number for a single hidden layer .In a single hidden layer network, the number of neurons in the hidden layer determines the number of hyper planes portraying the function. If the number of hyper planes (i.e. neurons in the hidden layer) is sufficient, they can form complex arbitrary shapes, matching the function. Contrarily, if they are too few, they will only follow the main trends and the representation of the function will be poor, as illustrated in Figure 1.2.

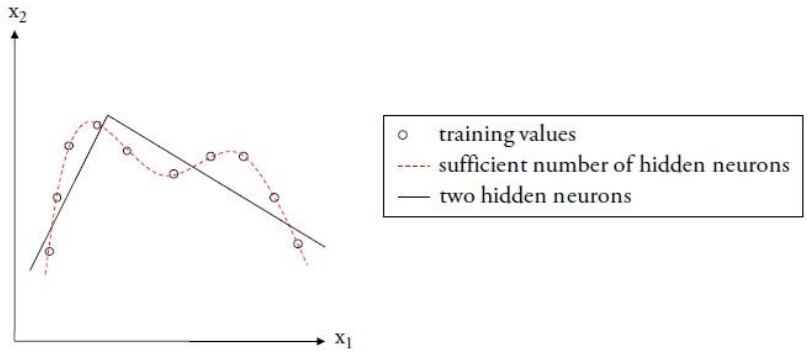

Figure 1.2 Regression with too few hidden neurons [8].

Too many neurons in the hidden layer will, on the other hand, result in an over fitted network with bad generalization capabilities, as demonstrated in Figure 1.3.

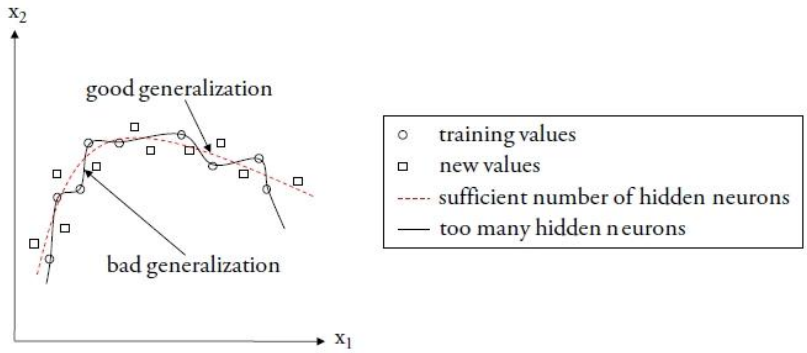

Figure 1.3 Regression with too many hidden neurons [8].

When conducting this trial-and-error process of choosing an appropriate number of hidden neurons, it is wise to start with a low number, and increase it until satisfactory results are achieved [8].

3. Transfer function in neurons

The transfer function in neurons is chosen depending on the task at hand. Two commonly used transfer functions, or activation functions, in multi-layer perceptron (MLPs) are the hyperbolic tangent and logistic functions. Two important aspects concerning modeling non-linear systems and using MLPs are the differentiability of the transfer function and the inclusion of non-linear parts, both of which are fulfilled by the hyperbolic tangent and logistic function [8].

4. Error criterion

The error criterion, or cost function, is a function of the error that needs to be minimized in order to improve a network's performance. In supervised training, the error can either be defined directly by the difference between the desired output and the actual output, or by a function of the error. When training MLPs, it is common to employ the mean squared error (MSE), which is the sum of the square difference between the desired response and the actual output. The MSE is minimized by changing the weights according to the training algorithm and, if the MSE reaches zero, the network output matches the desired outputs [10].

5. Training algorithm

The training algorithm, most commonly used together with MLPs, is the back-propagation training algorithm, also known as the generalized delta rule (see Chapter 2.1.2). The learning is based on an error criterion that is minimized with respect to the weights in the network. The challenge, as compared to the training of a single-layer network, is that no information concerning target values can be

obtained from the neurons in the hidden layer. In other words, if an output unit produces an incorrect response when the network is presented with an input vector, here is no way of knowing which of the hidden units is responsible. Consequently, it is impossible to know which weight to adjust, and by how much [8].

6. Stop criteria

The stop criteria can be used to avoid overtraining through the application of a cross-validation method. The cross-validation method involves measuring the network's performance during training and, if any incentive is given, stop the training before the maximum number of iterations (epochs) is reached. This is done by splitting the data set into two parts, one training data set and one cross-validation data set.

The training data set is used to calculate the errors and is thereby a part in the process of updating the weights. The cross validation data set is not directly used in the training, but continuously verifies the networks performance with independent patterns during the training procedure. If the error (e.g. MSE) based on the cross-validation data set starts to increase, as the error based on the training data set continues to decrease, it is an indication of overtraining [8].

7. Initial values of weights

The initial values of weights are normally set by randomization since no analytical solution is available. Nevertheless, certain aspects are worth considering. The initial values should be in a range so that the input to the transfer function is kept out of the saturated region. It is also of interest that the neurons learn at the

same rate, which can be accomplished by providing them with equal starting conditions [10].

ANN is very similar to biological neural network. ANN is composed of a group or groups of mathematically connected neurons. A single neuron connected many other neurons. The connections are usually formed from weight to bias on any function. Input data go through the weight and bias, and then it worked out using the function. ANN can obtain an optimized relation between the dependent and independent variables. Neural network has powerful advantages: 1) can resolve a non-linear problem. 2) learns and trains itself and does not need to be reprogrammed. 3) can continue without any problem by their parallel nature.

1.4 Overview of present works

Lefebvre A. H. and Perez R. studied fuel effects on gas turbine combustion-liner temperature and pollutant emissions [11]. Ouimette P. and Seers P. studied NOx emission characteristics on partially premixed flames using syngas (H_2/CO/CO_2 mixture) [12]. Continuous emission monitoring (CEM) and Predictive emissions monitoring (PEMS) already have made good use of monitoring malfunction of hardware on line. The CEM and PEMS are integrated artificial neural network (ANN) system.

Ilamathi P. et al. had shown an approach to model combustion process to predict and minimize unburned carbon in coal-fired boiler used in thermal power plant. They studied the effect of excess air, coal properties, boiler load, air distribution scheme, and nozzle tilt. As well, artificial neural network was applied to model the unburned carbon in bottom ash. They offered an alternative for engineers to evaluate the effect of operational parameters on carbon burnout behavior when coal switching happened [13].

Chatzopoulos A. K. et al. investigated a chemistry tabulation approach using artificial neural networks with turbulent non-premixed CH_4/H_2/N_2 flames. They proposed a chemistry tabulation approach based on Rate-Controlled Constrained Equilibrium (RCCE) and Artificial Neural Networks (ANNs) and apply it to two non-premixed and non-piloted, CH_4/H_2/N_2turbulent flames. The results indicated that the RCCE-ANN approach has potential to provide efficient techniques for incorporating comprehensive chemistry in probability density function (PDF) modeling [14].

Surajdeen A. I. et al. inspected the prediction of NOx as well O_2 for a model of furnace of an industrial boiler using an artificial neural network. The studied boiler is 160MW, gas fired with natural gas, water tube boiler and having two vertically aligned burners. They used data of computational fluid dynamics for the combustor. As well, they provided an efficient RBF network soft sensing solution to the problem of on-line monitoring of NOx emission from the boilers. Prediction of NOx is essential to monitor the emission level, while O_2 is an indicative of the burning efficiency of the fuel [15].

Fast M. et al. had created an online system for condition monitoring and diagnosis of a combined heat and power plant in Sweden. They selected input parameters; steam flow HRSG, Steam flow boiler, steam temperature boiler etc., output parameter; power output, FW temperature and condenser heat. As well, they developed artificial neural network model and optimized the plant operations and maintenance [16].

Chandrasekaran N. and Guha A. studied the prediction method for NOx emission from turbofan engines. To control aircraft emission, they investigated an accurate tool for predicting emissions. They applied generic method which compare well with the most dependable method. As well, they compared their results with previous studies. There are many list of correlation based method as follow appendix A.

However, NOx prediction or correlation has not yet been studied for $H_2/CO/CH_4$ syngas in the partially premixed model gas turbine. To reduce flashback probability of syngas, partially premixed combustors have been

utilized. Nevertheless, mixing length is not shot to reduce NOx emissions still. So, NOx emissions are remained issue in industrial power plant, aviation industry etc. To reduce NOx concentration, NOx generation mechanism should be investigated. However, NOx prediction or correlation has not yet been studied for H_2/CO/CH_4 syngas in the partially premixed combustor.

In this study, we conducted experiments under various operating conditions with a model gas turbine combustor to examine the relation of NOx concentration and flame structure using the OH*, CH* and C_2* chemiluminescence and artificial neural network. The result of this study strongly suggests that the flame temperature and flame length contribute to the NOx concentration. As well, OH*, CH* and C2* chemiluminescence overlapped image is more accurate than OH* chemiluminescence image only for H2/CO/CH4 various syngas composition.

Chapter 2 APPARATUS AND EXPERIMENTAL METHOD

2.1 Model gas turbine combustor

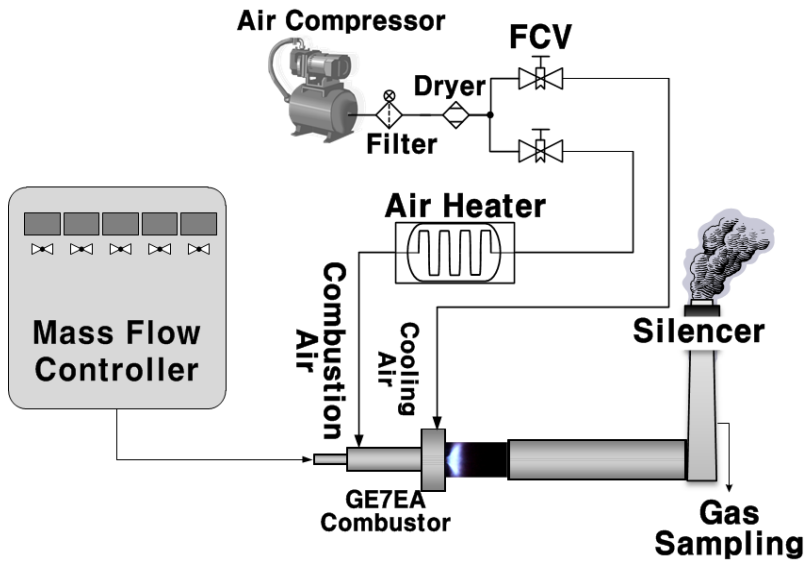

Figure 2.1 Schematic of model gas turbine combustor.

Figure 2.1 shows a schematic of a premixed, variable length, model gas turbine combustor. It consists of an air heater, a swirl injector, an optically accessible quartz combustor section, a mass flow controller and an exhaust duct. The air heater can heat air up to about 1300K and provide the heated air to the combustor through the air inlet part. There is a choking orifice at the entrance of the air inlet section to provide a well-defined acoustic boundary condition and to protect the fluctuation of inlet air. Before the combustion zone, injector can mix fuel and air.

The combustor consists of a stainless steel dump plane, an optically accessible quartz combustor, and a steel combustor. The downstream end of the quartz combustor is connected to a stainless steel variable-length combustor section. The length of the steel combustor can be varied continuously from 850 mm to 1100 mm by moving a water-cooled plug nozzle along the axial direction of the combustor. Mass flow controller can control fuel flow rate and air flow rate. As well, it can mix each fuel before entering the inlet section.

To measure the temperature on the combustion environment, four K-type thermocouple eleven dynamic pressure sensors (PCB 102A05) are equipped. Figure 2.2 shows location of the sensing point.

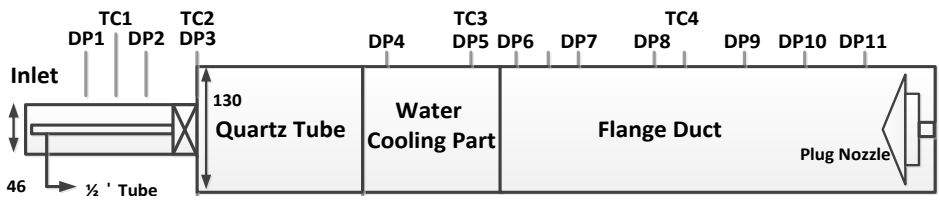

Figure 2.2 Location of dynamic pressure sensor and thermocouple.

2.2 Swirl injector

In order to examine the combustion characteristics of the syngas, 1/3 scaled downed one-can combustor of GE 7EA gas turbine is designed. Swirl flows have been studied in practical combustion systems such as industrial burners, furnaces, gas turbines for their high energy conversion in a small volume. When fuel-air mixture swirl in the combustion zone, flame hold up stable state and settled ignition behavior wide operation range. Because, high swirl number promotes well mixing, flammability limits, shortening flame length and reducing pollutant emissions [17]. Therefore, swirl injector has many advantages for gas turbine combustor.

Fuel injection and mixing are critical to achieve efficient and clean combustion in gas turbine engines, whether they are powered by gaseous or liquid fuels. For gaseous fuel, the most important thing is to get an optimal level of mixing among the air, fuel, and combustion products in the combustion zone [18]. The variable control parameter, swirl angle and number of swirl vane, is very important factor for gas turbine operation conditions

In this study, the axial-entry type swirl injector was used as a fuel feeding device and a fuel/air mixer. In the axial-entry type swirl injector, the flow is deflected by an array of vanes positioned axially, as illustrated in Fig 2.3 and Fig 2.4

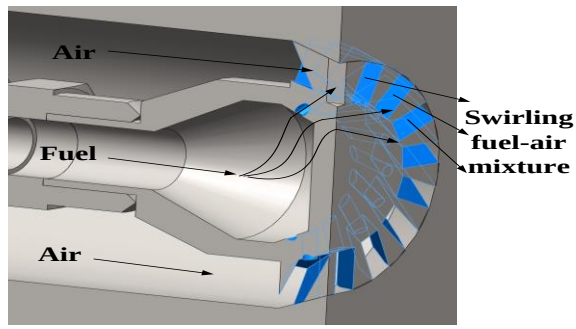

Figure 2.3 Schematic of the axial entry type swirl injector.

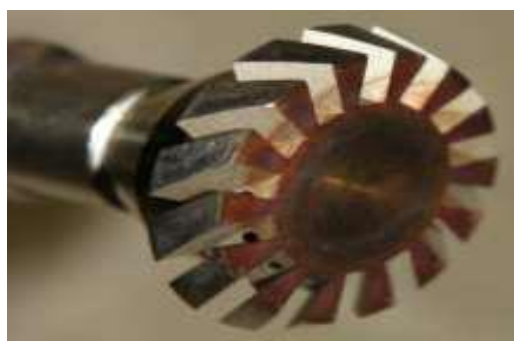

Figure 2.4 Direct photo of the test fuel nozzle

Fuel-air mixture is supplied through the annually arranged 14 swirl vanes of which the angle is 45 degree and fuel is injected within the swirl vane at about 2.7mm up-steam of dump plane to make partially premixed flame. Inner and outer diameter of swirl vane is 25.5mm and 40mm respectively.

The most important parameter in swirl flow is the swirl number that indicates the swirl intensity. It is defined as the ratio of the axial flux of the tangential momentum to the product of the axial momentum flux and a characteristic radius [19]. The exact expression of swirl number depends on the injector geometry and

flow profiles. If the axial and tangential velocities are assumed to be constant and swirl vanes are thin enough, swirl number S_n could be calculated by equation (2.1)

$$S_n = \frac{2}{3}\left[\frac{1-(D_{swirl-in}/D_{swirl-out})^3}{1-(D_{swirl-in}/D_{swirl-out})^2}\right] tan\varphi \qquad (2.1)$$

D_{swirl_in}, D_{swirl_out} and φ are inner diameter of swirler, outer diameter of swirler and swirl vane angle, respectively. According to the equation, swirl number is about 0.83 [20].

2.3 Chemiluminescence detection system

A high-speed ICCD Camera (as shown Fig 2.6) was used in this study for recording flame images through quartz. For obtaining chemiluminescence images, three optical band pass filter was applied. The specifications for each of the optical interference filters are as follows Fig 2.5 and Table 2.1.

Figure 2.5 Optical interference band-pass filters; OH*, CH* and C_2*

Optical filter	Center of wavelength	Band-pass wavelength
OH*	307.1 nm	15 nm
CH*	430.0 nm	10 nm
C_2*	515.0 nm	10 nm

Table 2.1 Specifications of optical interference filter

OH*, CH* and C_2* intensities are investigated to correlate with the heat release rate in the flame for particular equivalence ratios. It is also useful to understand the flame front structure by local chemiluminescence intensity. The OH* radical intensity is not only related to the main flame temperature but also associated to

reaction rate and heat release rate. The CH* radical emission reacts strong in the flame front in slightly rich conditions close to fuel stream; it characterized the hydrocarbon and NO reactions. The C_2* radical intensity relates bands with rich flames.

Figure 2.6 Princeton instrument PI-MAX 2 (16bit ICCD)

2.4 Test condition

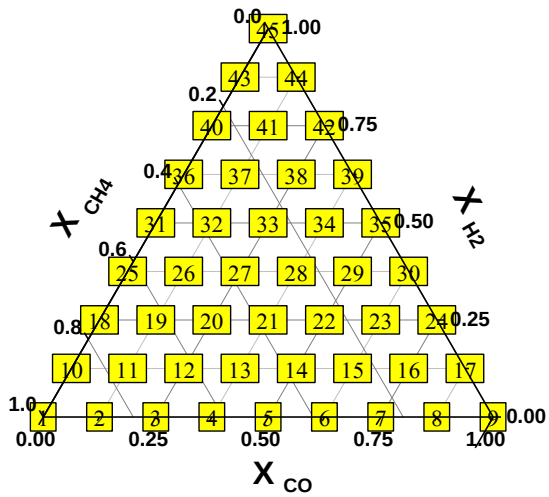

Figure 2.7 Ternary diagrams for H_2/CO/CH_4 syngas

Fig 2.7 shows the ternary diagrams for H_2/CO/CH_4 syngas. For investigating H_2/CO/CH_4 syngas combustion characteristics, each species mole fraction was changed from 0% to 100% at varying 12.5%. A total of experiment condition was 45 cases. For example, number 27 case consist of hydrogen 37.5%, carbon monoxide 25.0% and methane 37.5%. In this ternary diagrams, experimental conditions (number 1, 18, 20, 31, 33 and 40) is that external recirculation zone was observed and the flame was stable combustion conditions. Therefore, those experimental conditions was selected for investigated characteristics of varying equivalence ratio and emission trend and the equivalence ratio of 0.7 to 1.3 at increments of 0.1 was performed. Air mass flow rate was changed from 490 to 1,100 for varying equivalence ratio at fixing fuel flow rate.

Parameter	Values
Fraction	Molecular basis
Fuel	H_2/CO/CH_4
Heat input [kW]	50
Air temperature [K]	30
Combustor length [mm]	1410
Air mass flow rate [slpm]	490~1100
Equivalence ratio	0.7~1.3

Table 2.2 Experimental condition

As shown Table 2.2, heat input was 50kW, inlet air temperature was about 300K, combustor length was 1410mm from combustor dump to plug nozzle.

Through this process, flame length trend, flame temperature characteristics and emissions characteristics can be investigated.

Chapter 3 RESULTS AND DISCUSSION

3.1 NOx characteristics

TESTO 360 gas analyzer was used in this study for NOx concentration. The NOx average measured value for 30 seconds was obtained. As well, thermocouple 3 (as follow Fig 2.2) can be represented the flame temperature. NOx concentrations and flame temperature characteristics were investigated at varying equivalence ratio.

Fig 3.1 and Fig 3.2 is NOx concentrations and Flame temperatures with respect to equivalence ratio, respectively. In general, maximum value of NOx concentration and flame temperature is occurred near equivalence ratio 1.0. At varying fuel compositions, while hydrogen composition increased, NOx concentrations and flame temperatures increased. Because hydrogen has more higher heating value than methane and carbon monoxide. (Lower heating value; hydrogen: 28,670kcal/kg, carbon monoxide: 2,415kcal/kg, methane: 11,955kcal/kg)

Therefore, flame temperature increase with high hydrogen compositions. NOx concentration is the function of flame temperature, also. Thus, NOx centration and flame temperature characteristics appeared similar trend. However, the maximum temperature was at slightly rich equivalence ratio. It is a consequence of both the heat of combustion and heat capacity of the products declining beyond Φ=1. For equivalence ratios between Φ=1 and Φ (T_{max}), the heat capacity decreases more rapidly with Φ than ΔH_c; while beyond Φ(T_{max}), ΔH_c falls more

rapidly than does the heat capacity. The decrease in heat capacity is dominated by the decrease in number of product moles formed per mole of fuel burned, with the decrease in the mean specific heat being less significant [2].

From these results, NOx characteristics can be obtained for H_2/CO/CH_4 syngas flame at varying equivalence ratio and fuel compositions.

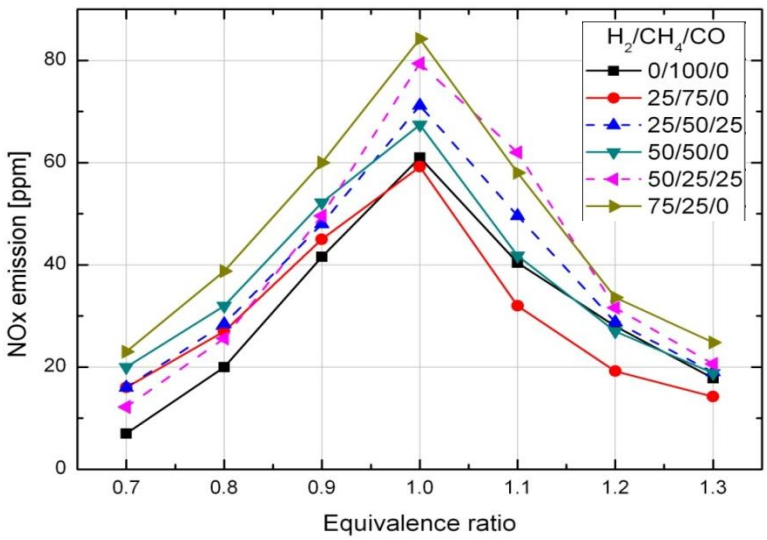

Figure 3.1 NOx concentrations with respect to equivalence ratio

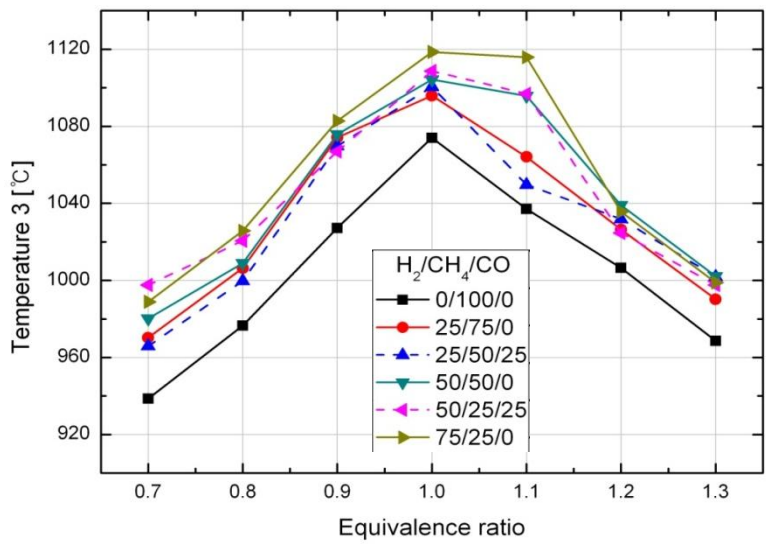

Figure 3.2 Flame temperatures with respect to equivalence ratio

3.2 Chemiluminescence and flame structure

A high-speed ICCD camera was used in this study for flame visualization. To obtain calculating of the exact flame area and length, OH*, CH* and C_2* chemiluminescence overlapped images are employed, because OH*, CH* and C_2* chemiluminescence varies a lot with respect to H_2/CO/CH_4 syngas composition. In case of only H_2 flame, CH* radical and C_2* radical cannot be measured. In contrast of CH_4 or CO flame, OH* radical may not release a lot. For obtain the OH*, CH* and C_2* radical characteristics each fuel compositions, each band-pass filters were equipped in front of ICCD camera lens. In addition, Abel-inversion process was used to take the 2-D images from accumulated 3-D flame images.

Table 3.1 is the each chemiluminescence image and flame area for H_2/CO/CH_4 fuel compositions. From Table 3.1, flame area from calculating chemiluminescence intensity varied with fuel composition and each chemiluminescence. Therefore, OH*, CH* and C2* chemiluminescence overlapped images were used to obtain exact flame area or length as shown in Table 3.2.

Fuel compositions	H_2/CO/CH_4 0%/100%/0% Φ=1.3	H_2/CO/CH_4 25%/50%/25% Φ=1.3	H_2/CO/CH_4 25%/75%/0% Φ=0.8
OH* image	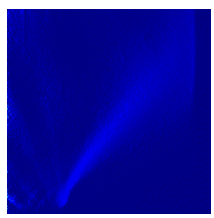	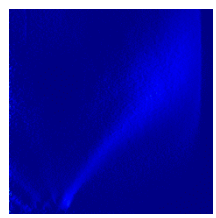	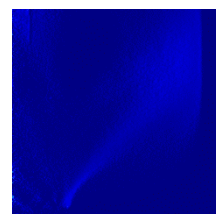
Flame area [cm^2]	6.62	6.74	6.43
CH* image	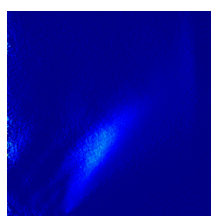	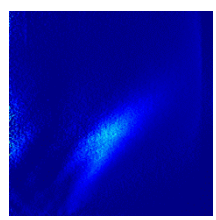	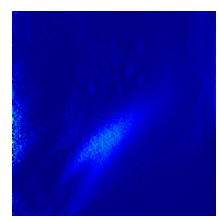
Flame area [cm^2]	7.99	8.64	7.54
C_2* image	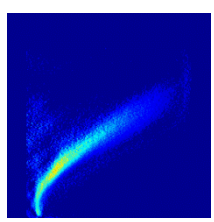	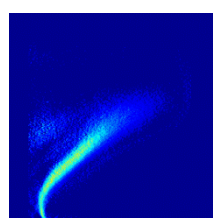	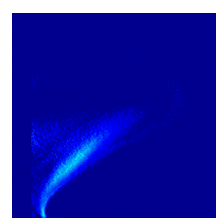
Flame area [cm^2]	7.34	7.19	6.01

Table 3.1 OH*, CH* and C_2* image and flame area for various fuel compositions.

Fuel compositions	H_2/CO/CH_4 0%/100%/0% Φ=1.3	H_2/CO/CH_4 25%/50%/25% Φ=1.3	H_2/CO/CH_4 25%/75%/0% Φ=0.8
OH*/CH*/C_2* overlapped image	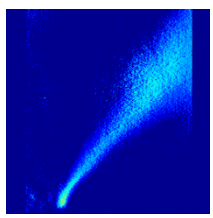	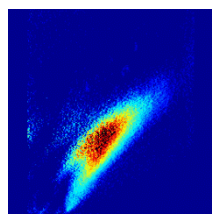	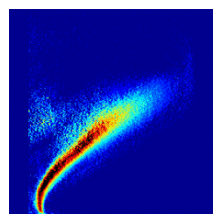
Flame area [cm^2]	6.85	9.07	7.60

Table 3.2 OH*, CH* and C_2* overlapped image and flame area for various fuel compositions.

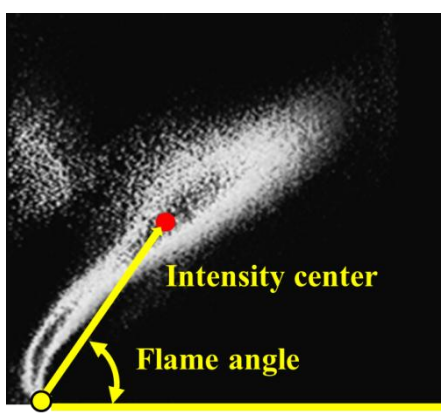

Figure 3.3 Definition of intensity center and flame angle.

To quantify the flame structure, the concept of the gravity center was used to calculate the flame center. The flame angle is computed from the intensity center and the center of the dump plane. In other words, the angle between the intensity center and the middle of the dump plane is regarded as the flame angle. This can be shown at Fig 3.3. Flame angle can demonstrate the axial and radial momentum ratio; a similar concept about flame center is used in the research of Kim et al [21]. flame angle is a factor that can represent the flow structure of the flame. The calculation for the flame center is performed in all phases of the Abel-inverted image.

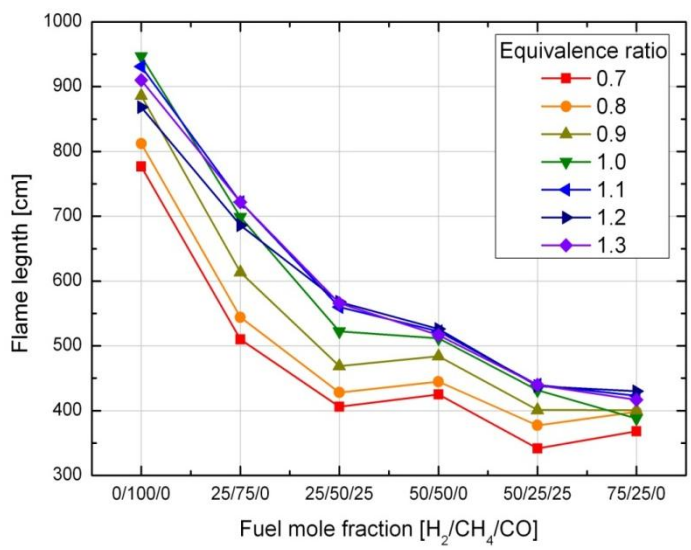

Figure 3.4 flame length with respect to various fuel compositions;

H_2, CO and CH_4.

Flame length defined the length from intensity center to mixture injecting hole. Fig 3.4 is the flame length characteristics with respect to fuel mole fraction of

H_2/CO/CH_4. From the graph, flame length decreases as increasing hydrogen composition. It is result from fast burning velocity of hydrogen. (Burning velocity; hydrogen: 289cm/s, carbon monoxide: 19cm/s, methane: 37 cm/s)

3.3 Emissions characteristics

As mentioned above, EINOx was investigated to find out the effect of NOx concentration in respect of burned fuel. According to previous work, EINOx is the function of flame length and flame temperature and so on. Oh J. et al. studied the effect of swirl flow on pollutant emission in a non-premixed turbulent hydrogen jet with coaxial air. They investigated that EINOx decreased with the swirl vane angle and increased with the flame length. As well, it increased in proportion to the flame residence time and the global strain rate [22]. In this study, EINOx was affected to flame temperature and flame length as shown in Fig 3.5~Fig 3.6.

From the graphs, EINOx increases as increasing the flame temperature which was measured in 3rd thermocouple as shown in Fig 2.2. In addition, equivalence ratio affects EINOx characteristics. EINOx in other words NOx is the function of flame temperature. NOx is proportional to flame temperature. As well, EINOx increases as increasing equivalence ratio in fuel lean condition. In contrast, EINOx decreases as increasing equivalence ratio in fuel rich condition. Maximum EINOx value occurred at Φ=1. Besides, EINOx increases as increasing the reciprocal of flame length which was defined above chapter 3.2 and it is shown in Fig 3.7~Fig 3.8.

Through in Fig 3.5~Fig 3.8, EINOx is affected locally generated high flame temperature in a compact burning flame. It is contrast result against diffusion jet flame EINOx characteristics. It is caused from the difference combustion mechanism between premixed combustion and diffusion combustion. In diffusion

flame, NOx generates outer line of the flame, because stoichiometric condition occurs at edge of the flame. Most NOx concentration generates the highest temperature area that is stoichiometric state. In contrast of diffusion flame, NOx concentrates in the broad combustion zone at premixed flame. Before igniting the flame in the combustion zone, fuel and air mixed well. Therefore, most of the flames maintain the stoichiometric condition. Consequently, locally high temperature in a short flame affects EINOx concentration.

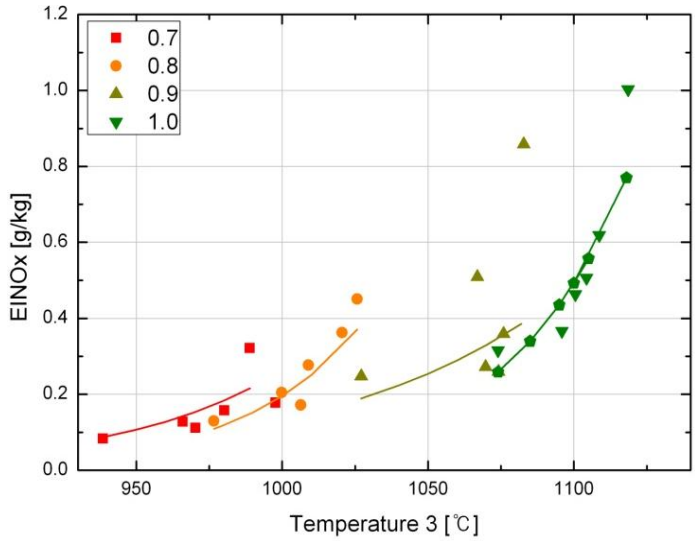

Figure 3.5 EINOx with respect to flame temperature at fuel lean condition.

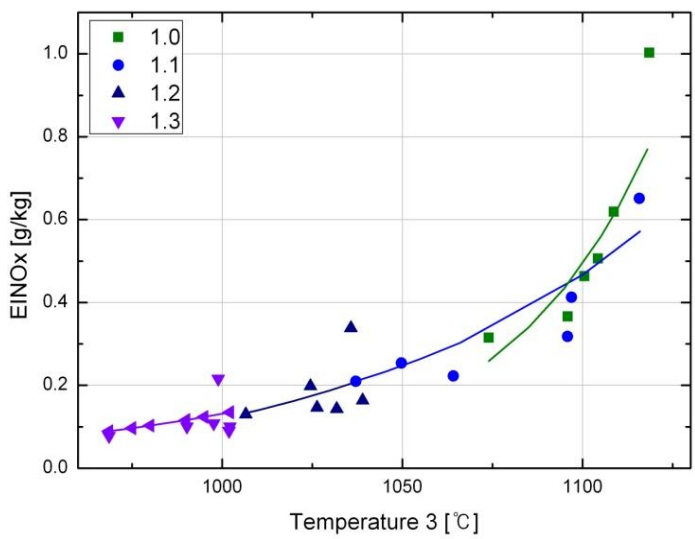

Figure 3.6 EINOx with respect to flame temperature at fuel rich condition.

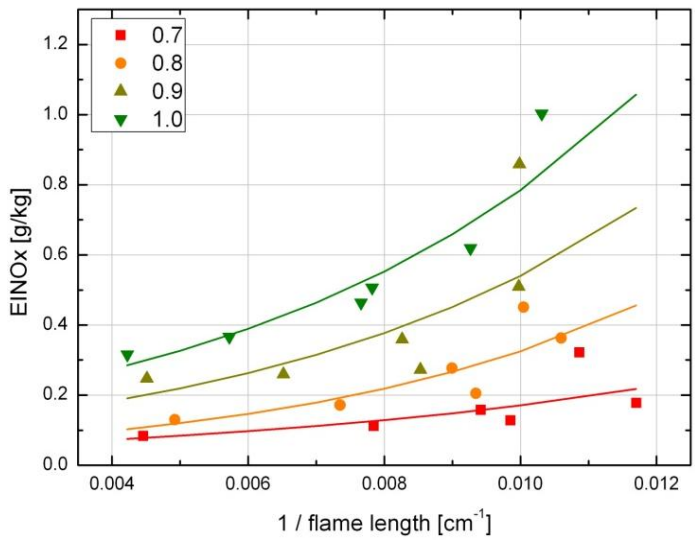

Figure 3.7 EINOx with respect to the reciprocal of flame length at fuel lean condition.

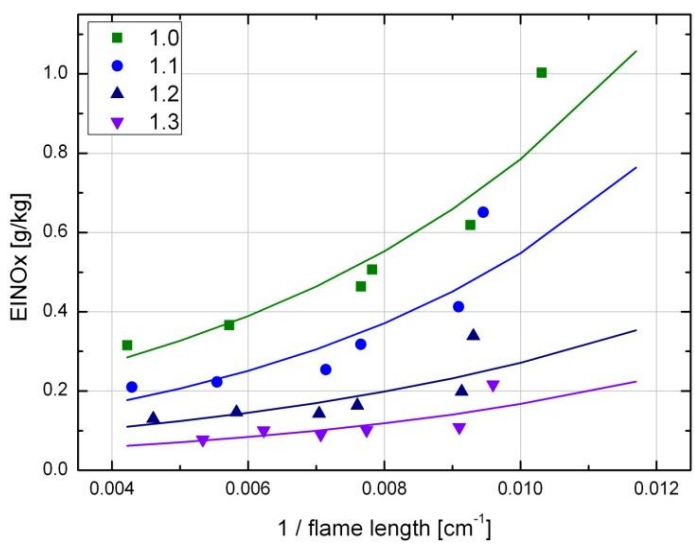

Figure 3.8 EINOx with respect to the reciprocal of flame length at fuel rich condition.

3.4 Emissions estimation

Laviolette M. et al. reformed the EINOx equations of Lefebvre A.H. et al. and Odger J. et al. to improve accuracy [23]. As well, they applied the correlation coefficient (R^2) to judge the reliability between estimated values and measured values as shown in equation (3.1)~(3.3).

$$EINOx = 7.039 \times 10^{-8} \frac{P_3^{0.9854} V_c exp(0.0081 T_{st})}{\dot{m}_A T_{pz}} \tag{3.1}$$

$$EINOx = 1.902 \times 10^{5} \frac{P_3^{0.4048} \left[1 - e^{(-480\tau)}\right]}{e^{\left(\frac{37902}{T_{st}}\right)}} \tag{3.2}$$

$$R^2 = \frac{[\sum_i (x_i - \bar{x})(y_i - \bar{y})]^2}{\sum_i (x_i - \bar{x})^2 \cdot \sum_i (y_i - \bar{y})^2} \tag{3.3}$$

Artificial neural network was applied to estimate EINOx establishing input parameters pressure in the combustion chamber, flame residence time and stoichiometric adiabatic flame temperature and 5 neurons. As the results, they investigated EINOx modeling and the correlation coefficient was 0.87. In this study, artificial neural network was investigated to know the effect of any input parameters to predict EINOx.

3.4.1 Exhaust gas concentration

Most published models are based on knowledge of the physics and chemistry that is thought to be ongoing in the combustion chamber. For this reason they are mostly semi-empirical and not simply correlations of measured date. According to Lefebvre A.H. et al., three processes are deemed to be important: the mean residence time, the chemical reaction rate and the mixing rate [11,23].

1. Residence time

Residence time is that the amount of NOx produced is much smaller than the chemical equilibrium values for the temperature in the primary zone [24]. If equilibrium is not reached, an average residence time is required to evaluate, from the reaction rate, the amount of NOx produced. The expressions for residence time is shown in equation (3.4)

$$\tau \propto \frac{PV}{\dot{m}_A R_{air} T_{pz}} \tag{3.4}$$

T_{pz} is the combustion chamber inlet temperature, R_{air} is the ideal gas constant for air, m_A is the mass flow rate of air and V is the volume of the combustion zone.

2. Chemical reaction rate

It assumed that an Arrhenius form of reaction rate equation must be used because a series of chemical reactions is producing the NOx. In most gas turbine combustion chambers, this happens in the primary zone where there is a jet flame and therefore the adiabatic flame temperature of a stoichiometric mixture is investigated. The expressions for chemical reaction rate are shown in equation (3.5) [23].

$$\text{Chemical reaction rate} \propto P^{m} e^{ZT} \tag{3.4}$$

3. Mixing rate

The mixing rate depends on the aerodynamics of the combustion chamber and is driven by pressure forces. For cycle efficiency reasons, the allowable pressure drop within the combustion chamber limits the mixing rate. The ratio of total pressure drop across the combustion chamber to inlet pressure of the chamber may be as low as 2.5% in industrial applications [23].

In this study, variable parameters are flame length (L_{flame}), flame temperature (T_{pz}) and air flow rate (m_A) for all experimental conditions. The variable for premixed combustion of syngas flame can be compared with Lefebvre et al.'s theory. Besides, it can be displayed NOx concentration in diagram form as shown Fig 3.9.

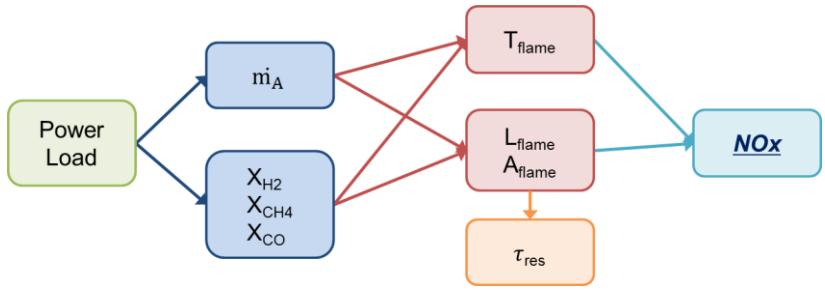

Figure 3.9 Diagram for NOx concentration in applications.

Fuel and air is decided for consumer to want power load and flame temperature and flame length is determined with respect to the fuel and air flow rate. Flame residence time relate to the flame length for flame area. Finally, NOx concentration is set by these parameters. In other words, flame temperature, flame length, fuel flow rate and air flow rate can affect the NOx concentration for gas turbine combustion.

3.4.2 ANN modeling

As mentioned above, artificial neural network is the tool for predicting any processes. It is very important to select the input parameter, number of neurons, transfer function to liaise between neurons, etc. In this study, input parameter was established to the flame length from inverted chemiluminescence images, flame temperature from 3rd thermocouple and air mass flow rate. As well, to compare the only OH* chemiluminescence image with OH*, CH* and C_2* chemiluminescence overlapped image, artificial neural network set up for these cases. Levenberg-Marquardt algorithm was used to reduce the difference estimated EINOx with measured EINOx. Validation set was 15% of the overall set and removed randomly form the overall set. The validation set was not presented to the artificial neural networks during training or testing but was not presented to the ANN after training as an independent verification of the ANN's ability to predict [23]. Fig 3.10 and Fig 3.11 are the more detail structures of the ANN modeling for using OH* chemiluminescence images and OH*, CH* and C_2* chemiluminescence images to estimate EINOx concentration.

- MSE = 0.26
- Neuron = 21
- Epoch = 15

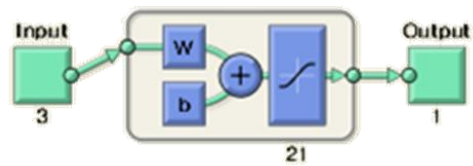

Fig 3.10 ANN structure as to OH* chemiluminescence images

- MSE = 0.18
- Neuron = 29
- Epoch = 12

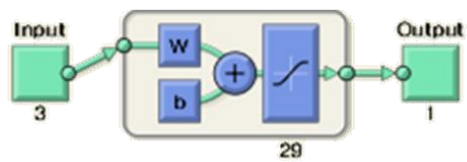

Fig 3.11 ANN structure as to OH*, CH* and C_2* chemiluminescence images

Fig 3.10 is the ANN structure for using OH* chemiluminescence images. 21 neurons were used at minimum error between estimated EINOx and measured EINOx, mean squared error was 0.26 and iteration number was 15. In contrast, Fig 3.11 is the ANN structure for using OH*, CH* and C_2* chemiluminescence images. 29 neurons were used at minimum error between estimated EINOx and measured EINOx, mean squared error was 0.18 and iteration number was 12. ANN modeling for using all chemiluminescence images is more accurate result than using only OH* chemiluminescence images. As the result, flame length for using OH*, CH* and C_2* overlapped chemiluminescence image is more accurate for syngas combustion.

The predicted values vs. measured values were plotted on a decimal scaled and are shown in Fig 3.12 and Fig 3.13. Compared to the two other correlations the

data are well estimated by the chosen ANN. The coefficients of determination of the prediction for all models are 0.62 for OH* chemiluminescence images and 0.78 for OH*, CH* and C_2* chemiluminescence overlapped images. Weight matrix and bias matrix for two other ANN modeling will be omitted. To verify the weight of the input parameter, weight matrix and bias matrix should be calculated. As the results, the effectiveness of EINOx emissions is order of flame temperature (41%), flame length (34%) and air mass flow rate (25%).

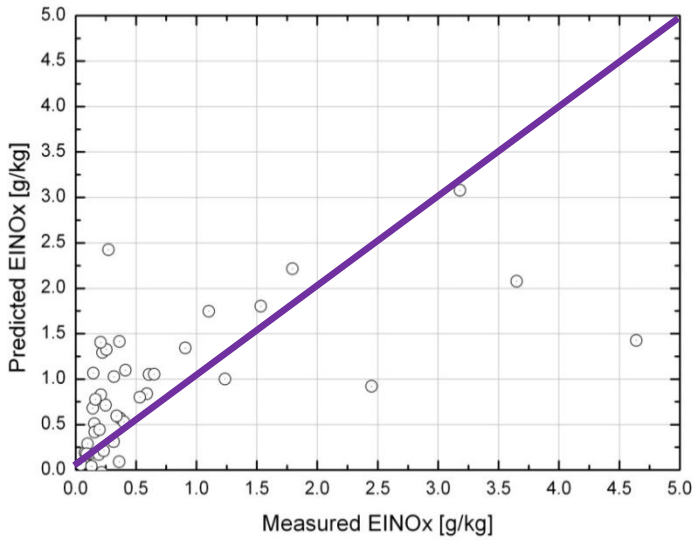

Figure 3.12 Comparison of EINOx predicted by the present work to measured values using OH* images

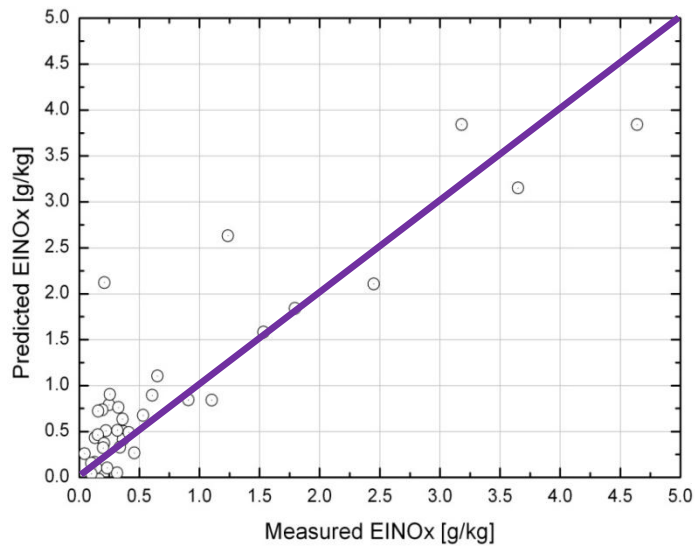

Figure 3.13 Comparison of EINOx predicted by the present work to measured values using OH*, CH* and C_2* images

Chapter 4 CONCLUSION

A comprehensive set of experiments was performed to investigate the flame length characteristics, emissions characteristics and apply artificial neural network to estimate the EINOx in model gas turbine combustor for $H_2/CO/CH_4$ syngas. From the experimental results, we look into the NOx generating mechanism using chemiluminescence image.

EINOx emission for $H_2/CO/CH_4$ syngas fuel on partially premixed combustion relates the flame characteristics. EINOx is affected locally generated high flame temperature in a compact burning flame. It is contrast result against diffusion jet flame EINOx characteristics. It is caused from the difference combustion mechanism between premixed combustion and diffusion combustion. In diffusion flame, NOx generates outer line of the flame, because stoichiometric condition occurs at edge of the flame. Most NOx concentration generates the highest temperature area that is stoichiometric state. In contrast of diffusion flame, NOx concentrates in the broad combustion zone at premixed flame. Before igniting the flame in the combustion zone, fuel and air mixed well. Therefore, most of the flames maintain the stoichiometric condition. Consequently, locally high temperature in a short flame affects EINOx concentration. It can be schematized follow Fig 4.1.

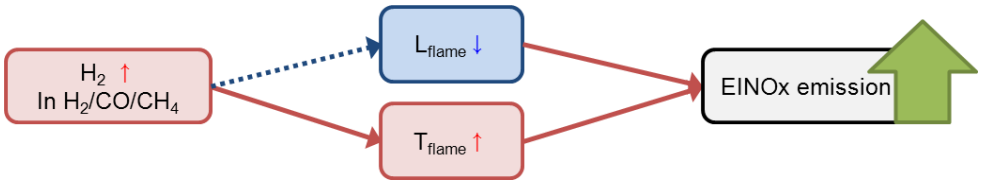

Figure 4.1 Diagram of relation between EINOx concentration and flame structure

Artificial neural network was applied to predict the EINOx emissions. From the ANN modeling results, flame length for using OH*, CH* and C_2* overlapped chemiluminescence image is more accurate to estimate the EINOx for H_2/CO/CH_4 various syngas compositions. Compared to the two other correlations the data are well estimated by the chosen ANN. The coefficients of determination of the prediction for all models are 0.62 for OH* chemiluminescence images and 0.78 for OH*, CH* and C_2* chemiluminescence overlapped images. In addition, the effectiveness of the EINOx concentration is order of flame temperature (41%), flame length (34%) and air mass flow rate (25%). From the results, flame temperature and flame length are important parameter for modeling artificial neural networks.

Appendix A. NOx Prediction Method Available in the Open Literature [25]

A.1 List of Correlation Based Models

1) For Rizk and Mongia (Eq. 2 in [26]),

$$EINOx = \frac{15 \times 10^{14} t_{res}^{0.5} exp\left(\frac{-71{,}100}{T_{fl}}\right)}{P_3^{0.03}\left(\frac{\Delta P_3}{P_3}\right)^{0.5}}$$

2) For Lipfert (Eq. B4 in [27]),

$$EINOx = 0.17282 \cdot \exp(0.006766593 T_3)$$

3) For AECMA (Eq. B15 in [27]),

$$EINOx = 2 + 28.5\sqrt{\frac{P_3}{3{,}100}}\, exp\left(\frac{T_3 - 825}{250}\right)$$

4) For Becker et al. (as cited in [28]),

$$NOx(ppmv) = 5.73 \times 10^{-6} \cdot \exp(0.00833 T_{fl}) P_3^{0.5}$$

5) For GasTurb [29],

$$S_{NOx} = \left(\frac{P_3}{2{,}965}\right)^{0.4} exp\left(\frac{T_3 - 826}{194} + \frac{6.29 - 100 \cdot \mathrm{WAR}}{53.2}\right)$$

6) For Dopelheuer and Lecht (Eq. 3 in [30]),

$$EINOx = EINOx_{SL}\left(\frac{P_{3_{FL}}}{P_{3_{SL}}}\right)^{0.5}\left(\frac{T_{3_{SL}}}{T_{3_{FL}}}\right)^{0.5}\left(\frac{T_{pz_{SL}}}{T_{pz_{FL}}}\right)^{0.5} \times exp\left[38{,}000\left(\frac{1}{T_{fl_{SL}}}-\frac{1}{T_{fl_{FL}}}\right)\right]$$

7) For Odger and Kretchmer (Eq. 9.8 in [11]),

$$EINOx = 29 \cdot \exp\left(\frac{-21{,}670}{T_{fl}}\right)P_3^{0.66}\left[1-exp\left(-250t_{form}\right)\right]$$

8) For Lefebvre (Eq. 1 in [31]),

$$EINOx = 4.59 \times 10^{-9} \cdot P_3^{0.25} \cdot F \cdot t_{res} \cdot exp\left[0.01\left(T_{fl}+273\right)\right]$$

9) For Blazowski (Eq. 11 in [32]),

$$EINOx = 10^{\left[1+0.0032(T_3-581.25)\sqrt{\frac{P_{amb_{FL}}}{P_{amb_{SL}}}}\right]}$$

10) For NASA (Eq.1 in [33]),

$$EINOx = 33.2 \cdot \left(\frac{p_3}{432.7}\right)^{0.4} \cdot exp\left(\frac{t_3-459.67-1027.6}{349.9}+\frac{6.29-6.3}{53.2}\right)$$

11) For NPSS (Eq.1.4 in [34]),

$$EINOx = 0.068 \cdot P_3^{0.5} exp\left(\frac{t_3-459.67}{345}\right) \cdot \exp(H)$$

12) For Deidewig and Dopelheuer (Eq. 1 in [35]),

$$EINOx = EINOx_{SL(TO)} \cdot \frac{exp\left(\frac{135{,}000}{RT_{\lambda_{SL}}}\right)}{exp\left(\frac{135{,}000}{RT_{\lambda_{FL}}}\right)} \cdot \frac{P_{3_{FL}}}{P_{3_{SL(TO)}}} \cdot \frac{W_{a_{SL(TO)}}}{W_{a_{FL}}} \cdot \frac{T_{3_{SL(TO)}}}{T_{3_{FL}}}$$

$$where\ T_\lambda = 2{,}281\left[P_3^{0.009375} + 0.000178 P_3^{0.005}(T_3 - 298)\right].$$

A.2 P_3-T_3 Method

The P3-T3 method is described in [36]:

$$EINOx_{FL} = EINOx_{SL}\left(\frac{P_{3_{FL}}}{P_{3_{SL}}}\right)^n \left(\frac{FAR_{FL}}{FAR_{SL}}\right)^m exp(H)$$

$$where\ \mathrm{H} = 19(h_{SL} - h_{FL}).$$

A.3 Fuel Flow Methods

1) For BFFM2 [37,.38],

$$W_{f_{SL}} = W_{f_{FL}}\left(\frac{\delta_{amb}^{3.8}}{\delta_{amb}}\right) e^{0.2Ma^2}\ \&\ EINOx_{FL} = EINOx_{SL}\left(\frac{\delta_{amb}^{1.02}}{\delta_{amb}^{3.3}}\right)^{0.5} e^H$$

$$where\ \theta_{amb} = \frac{T_{amb}}{288.15}, \delta_{amb} = \frac{P_{amb}}{101.325}, and\ H = 19(h_{SL} - h_{FL}).$$

2) For the DLR fuel flow method [30],

$$W_{f_{SL}} = W_{f_{FL}}\left(\frac{\theta_i^{-0.5}}{\delta_i}\right)\ \&\ EINOx_{FL} = EINOx_{SL}\left(\delta_i^{0.4} \cdot \theta_i^3\right) e^H$$

$$where\ \theta_i = \frac{T_{amb}(1 + 0.2Ma^2)}{288.15}, \delta_i = \frac{P_{amb}(1 + 0.2Ma^2)^{3.5}}{288.15},$$

$$and\ H = 19(h_{SL} - h_{FL}).$$

Bibliography

[1] U.S. Environmental Protection Agency. “Nitrogen Oxides (NOx), Why and How They Are Controlled”, Technical bulletin, 1999

[2] Stephen R. Turns, “An introduction to combustion concepts and applications- 3rd edition”, McGraw-Hill international edition, USA, 2012

[3] SCR Committee of Institute of Clean Air Companies, “Selective Catalytic Reduction Control of NOx Emissions”, Technical report, 1997

[4] Yu-Chien Chien, “Development of a Chemiluminescence Diagnostic System for Combustion Measurements”, Master Thesis, 1996

[5] Docquier. N. and Candel, S., “Combustion Control and Sensors: A Review”, Progress in Energy and Combustion Science, 2002

[6] Higgins, B., McQuary,M.Q., Lacas, F., Rolon, J. C., Darabiha, N., and Candel, S., “Systemic Measurements of OH Chemiluminescence for Fuel-lean, High-pressure, Premixed, Laminar Flames”, Fuel, 2001

[7] McCarthy J., Minsky M. L., Rochester N., Shannon C. E., “A proposal for the Dartmouth Summer Research Project on Artificial Intelligence”, AI Magazine, 2006

[8] Magnus, F., “Artificial Neural Networks for Gas Turbine Monitoring”, Doctoral Thesis, 2010

[9] Arriagada J., “Introduction of Intelligent Tools for Gas Turbine Based, Small-Scale Cogeneration”, Thesis for Degree of Licentiate in Engineering, 2001

[10] Principe J. C., Euliano N. R., Lefebvre W. C., “Neural and Adaptive Systems:

fundamentals through simulations", Wiley New York, 2000

[11] Lefebvre A. H., Perez R., "Fuel Effects on Gas Turbine Combustion-liner Temperature Pattern Factor and Pollutant Emissions", Journal of Aircraft, 1984

[12] Ouimette P., Seers P., "NOx Emission Characteristics of Partially Premixed Laminar Flames of H_2/CO/CO_2 Mixtures", International Journal of Hydrogen Energy, 2009

[13] Ilamathi P., Selladurai V., Balamurugan K., "Modeling and Optimization of Unburned Carbon in Coal Fired Boiler Using Artificial Neural Network and Genetic Algorithm", Journal of Energy Resoursce Technology, 2013

[14] Chatzopoulos A. K., Rigopoulos S., "A Chemistry Tabulation Approach via Rate-Controlled Constrained Equilibrium (RCCE) and Artificial Neural Networks (ANNs), with Application to Turbulent Non-Premixed CH_4/H_2/N_2 Flames", Proceedings of the Combustion Institute, 2013

[15] Surajdeen A. I., Moustafa. E., Mohamed A. H., Ahmed A. A., "RBF neural network inferential sensor for process emission monitoring", Control Engineering Practice, 2013

[16] Fast M., Palme T., "Application of Artificial Neural Networks to the Condition Monitoring and Diagnosis of a Combined Heat and Power Plant", Energy, 2010

[17] P.M.Anacleto, E.C. Fernandes, S.I.Shtork, "Swril flow structure and flame characteristics in a model lean premixed combustor", Combust. Sci. and Tech., 2003

[18] Ying Huang, Vigor Yang, "Dynamics and stability of lean-premixed swirl-stabilized combustion", Progress in Energy and Combustion science, 2009

[19] F. H. Champagne, S. Kromat, "Experiments on the formation of a recirculation zone in swirling coaxial jets", Experiments in Fluids, 2000

[20] Chou T. and Oatterson D. J., “In-cylinder Measurement of Mixture Mal-distribution in a L-head Engine”, Combustion and Flame, 1995

[21] Kim M., Choi Y., Oh J., Yoon Y., “Flame Vortex Interaction and Mixing Behaviors of Turbulent Non Premixed Jet Flames under Acoustic Forcing”, Combustion and Flame, 2009

[22] Oh J, Hwang J., Yoon Y., “EINOx Scaling in a Non-premixed Turbulent Hydrogen Jet with Swirled Coaxial Air”, International Journal of Hydrogen Energy, 2010

[23] Laviolette M. and Strawson M., “On the Prediction of Pollutant Emission Indices from Gas Turbine Combustor Chambers”, Proceeding of ASME Turbo Expo, 2008

[24] Sjoblom B.G. and Odger J., “Factors Limiting Inlet Temperatures”, In 5th International Symposium on Airbreathing Engines, 1981

[25] Chandrasekaran N. and Guha A., “Study of Prediction Method for NOx Emission from Trubofan Engines”, Journal of Propulsion and Power, 2012

[26] Mongia, H., and Dodds, W., “Low Emissions Propulsion Engine Combustor Technology Evolution Past, Present and Future,” 24th Congress of the International Council of the Aeronautical Sciences, 2004

[27] Green, J. E., “Greener by Design: The Technology Challenge,” Aeronautical Journal, 2002

[28] Tsalavoutas, A., Kelaidis, M., Thoma, N., and Mathioudakis, K., “Correlations Adaptation for Optimal Emissions Prediction”, Proceeding of

ASME Turbo Expo 2007, 2007

[29] Kurzke, J., GasTurb 11., “A Program to Calculate Design and Off-Design Performance of Gas Turbines”, 2007

[30] Dopelheuer, A., and Lecht, M., “Influence of Engine Performance on Emission Characteristics,” Symposium on Gas Turbine Engine Combustion, Emissions and Alternative Fuels, 1998

[31] Rizk, N. K., and Mongia, H. C., “Semi Analytical Correlations for NOx, CO and UHCE missions,” Journal of Engineering for Gas Turbines and Power, 1993

[32] Mulder, T. J., and Ruijgrok, G. J. J., “On the Reduction of NOx- Emission Levels by Performing Low NOx Flights,” 26th Congress of the International Council of the Aeronautical Sciences Including the Eighth AIAA Aviation Technology, Integration, and Operations Conference, International Council of the Aeronautical Sciences Paper, 2008

[33] Daggett, D. L., “Water Misting and Injection of Commercial Aircraft Engines to Reduce Airport NOx”, NASA, 2004

[34] Allaire, D. L., “A Physics-Based Emissions Model for Aircraft Gas Turbine Combustors,” M.Sc. Thesis, Massachusetts Institute of Technology, 2006

[35] Gardner, R. M., Adams, K., Cook, T., Deidewig, F., Ernedal, S., Falk, R., Fleuti, E., Herms, E., Johnson, C. E., Lecht, M., Lee, D. S., Leech, M., Lister, D., Massi, B., Metcalfe, M., Newton, P., Schmitt, A., Vandenbergh, C., and Van Drimmelen, R., “The ANCAT/EC Global Inventory of NOx Emissions from Aircraft,” Atmospheric Environment, 1997

[36] Norman, P. D., Lister, D. H., Lecht, M., Madden, P., Park, K., Penanhoat, O., Plaisance, C., and Renger, K., “Development of the Technical Basis New

Emissions Parameter Covering the Whole Aircraft Operation", NEPAIR, 2003

[37] Baughcum, S. L., Tritz, T. G., Henderson, S. C., and Pickett, D. C., "Scheduled Civil Aircraft Emission Inventories for 1992: Database Development and Analysis," NASA CR 4700, 1996

[38] DuBois, D., and Paynter, G. C., "Fuel Flow Method 2," Society of Automotive Engineers, 2006

초 록

최근 에너지 안보 및 기후변화에 대한 높은 관심이 부각됨에 따라 세계각국에서는 청정석탄 이용 기술에 대한 연구개발 및 실증사업이 활발하게 이루어지고 있다. 그 중 큰 비중을 차지하는 사업인 석탄가스화 사업은 미국, 중국 등을 중심으로 실증사업이 이루어지고 있으며, 국내에서 또한 태안에 IGCC 발전소 건설이 진행, 개발 중에 있다. 석탄가스화 사업은 고체상의 연료인 석탄을 가스화한 후 탈황, 집진의 정제과정을 거쳐 깨끗한 합성가스를 연료로 전력을 생산하는 기술이다. 하지만 이러한 합성가스에 대한 연구가 많이 이루어져있지 않아, 실제 발전소의 운용률은 높지 않은 실정이다. 이를 개선하기 위하여 많은 노력이 있어왔으나 여전히 연소기부에서의 사고사례는 꾸준히 보고되고 있다.

본 연구에서는 수소, 일산화탄소, 메탄의 합성가스에 대한 연소특성을 파악하기 위하여 부분 예혼합 연소기에서 연소 실험을 수행하였다. 실제 연소환경을 모사하기 위하여 모델가스터빈 연소기를 제작하였으며, GE7EA 부분 예혼합 특성을 갖는 노즐을 사용하여 실험장치 구성을 하였다. 다양한 연료 조성에 대하여 OH*, CH* 그리고 C_2* 자발광의 특성을 각각 파악하였으며, 다양한 연료가 포함된 연소특성에서는 단순 OH* 자발광 이미지가 아닌 OH*, CH*, C_2* 자발광 이미지를 중첩시킨 이미지를 활용해야 함을 본 연구를 통해 알아냈다. 또한 아벨변환을 수행하여 3-D 정보가 누적된 자발광 이미지로부터 2-D 정보를 포함하는 화염 이미지 정보를 재구성하였다. 화염의 온도와 아벨변환을 거친 화염의 이미지를 통하여 배기 배출물인 NOx 특성이 어떠한

경향성을 갖고 배출이 되는지를 파악하였으며, EINOx 가 어떠한 인자에 영향을 받는지 파악하는 연구를 수행하였다. 인공신경망을 통하여 EINOx의 배출 특성을 예측하는 연구를 수행하였으며, OH* 자발광 이미지로부터 얻어낸 화염의 길이를 이용한 모델링과 OH*, CH*, C_2* 자발광 이미지로부터 얻어낸 화염의 길이를 이용한 모델링이 어떠한 차이를 보이는지 파악하는 연구를 함께 수행하였다. 또한 인공신경망 모델링을 통하여 어떠한 연소 조건 및 특성이 EINOx에 영향을 미치는지 파악하는 연구를 수행하였다.

주요어: 가스터빈, 인공신경망, 자발광, 화염구조, 아벨변환, EINOx
학 번: 2012-20708